ResearchGate

See discussions, stats, and author profiles for this publication at: https://www.researchgate.net/publication/5379105

Expansion of the Octarepeat Domain Alters the Misfolding Pathway but Not the Folding Pathway of the Prion Protein †

ARTICLE *in* BIOCHEMISTRY · JULY 2008

Impact Factor: 3.02 · DOI: 10.1021/bi800253c · Source: PubMed

CITATIONS
18

READS
3

3 AUTHORS, INCLUDING:

Carsten Korth
Heinrich-Heine-Universität Düsseldorf
120 PUBLICATIONS **2,857** CITATIONS

SEE PROFILE

Available from: Carsten Korth
Retrieved on: 01 February 2016

Expansion of the Octarepeat Domain Alters the Misfolding Pathway but Not the Folding Pathway of the Prion Protein[†]

S. Rutger Leliveld,[‡] Lothar Stitz,[§] and Carsten Korth*,[‖]

Institute for Molecular Biophysics (INB-2), Research Center Jülich, D-52425 Jülich, Germany, Institute of Immunology, Friedrich-Loeffler-Institute, 72076 Tübingen, Germany, and Department of Neuropathology, Heinrich Heine University of Düsseldorf, 40225 Düsseldorf, Germany

Received February 12, 2008; Revised Manuscript Received April 1, 2008

ABSTRACT: A misfolded conformation of the prion protein (PrP), PrP^{Sc}, is the essential component of prions, the infectious agents that cause transmissible neurodegenerative diseases. Insertional mutations that lead to an increase in the number of octarepeats (ORs) in PrP are linked to familial human prion disease. In this study, we investigated how expansion of the OR domain causes PrP to favor a prion-like conformation. Therefore, we compared the conformational and aggregation modulating properties of wild-type versus expanded OR domains, either as a fusion construct with the protein G B1 domain (GB1-OR) or as an integral part of full-length mouse PrP (MoPrP). Using circular dichroism spectroscopy, we first demonstrated that ORs are not unfolded but exist as an ensemble of three distinct conformers: polyproline helix-like, β-turn, and "Trp-related". Domain expansion had little effect on the conformation of GB1-OR fusion proteins. When part of MoPrP however, OR domain expansion changed PrP's folding landscape, not by hampering the production of native α-helical monomers but by greatly reducing the propensity to form amyloid and by altering the assembly of misfolded, β-rich aggregates. These features may relate to subtle pH-dependent conformational differences between wild-type and mutant monomers. In conclusion, we propose that PrP insertional mutations are pathogenic because they enhance specific misfolding pathways of PrP rather than by undermining native folding. This idea was supported by a trial bioassay in transgenic mice overexpressing wild-type MoPrP, where intracerebral injection of recombinant MoPrP with an expanded OR domain but not wild-type MoPrP caused prion disease.

Prion diseases are transmissible neurodegenerative diseases in several mammalian species that can be of sporadic, genetic, or infectious origin. The main examples are Creutzfeldt-Jakob disease (CJD)[1] in humans, bovine spongiform encephalopathy (BSE) in cattle, and scrapie in sheep (*1*). The crucial event in the molecular pathway of all prion diseases is the conformational conversion of normal, membrane-bound prion protein, PrP^{C}, to a pathogenic conformer, known as PrP^{Sc} (*1*). The latter forms the essential component of infectious prions, the agent through which prion disease is transmitted (*1, 2*). Therein lies the unique nature of this family of diseases: the ultimate basis for both their pathology and infectivity is the misfolding of a host protein without the need for nonhost (i.e., viral or bacterial) nucleic acids (*2*). Important aspects of prion conversion can be studied in vitro using purified recombinant (rec) PrP, which has been shown to have a highly diverse folding landscape, one that includes infectious PrP^{Sc}-like conformers (*3*).

Several mutations in the human PrP gene (PRNP) have been genetically linked to familial CJD and related diseases (*4*). Human genetic prion disease can be transmitted to nonhuman primates (*5*). One type of mutation corresponds to the insertion of up to nine additional octarepeats (ORs; see below) in PrP (*6*). It has been confirmed that the resulting expansion of the OR domain generates infectious prions (*7*). Two transgenic mouse models have been generated to investigate the biological effects of mutant PrP with such an expanded OR domain (PrP^{C}-expOR). These mice overexpress either full-length mouse (Mo) PrP with nine extra repeats [14 in total, Tg(PG14)] or bovine PrP with four extra ORs (*8, 9*). Although both mouse strains developed a neurodegenerative disorder, they failed to produce infectious prions (*8, 10*). Apparently, PrP^{C}-expOR generates neurotoxic

[†] This work was supported by a research grant (LE 2197/1-1 to S.R.L.) from the German Research Foundation (DFG) and grants from the VW Foundation and EU Research commission to C.K. (LSHB-CT-019090; NeuroPrion).

* To whom correspondence should be addressed: Department of Neuropathology, Heinrich Heine University Düsseldorf, Moorenstrasse 5, 40225 Düsseldorf, Germany. Telephone: +49-211-811 6153. Fax: +49-211-8117804. E-mail: ckorth@uni-duesseldorf.de.

[‡] Research Center Jülich.

[§] Friedrich-Loeffler-Institute.

[‖] Heinrich Heine University of Düsseldorf.

[1] Abbreviations: aFFFF, asymmetric flow field-flow fractionation; CD, circular dichroism; CJD, Creutzfeldt-Jakob disease; CDSSTR, modified version of the variable selection method for deconvolution of CD spectra; exp, expanded; wt, wild-type; OR, octarepeat; PrP, prion protein; PPII, polyproline helix type II; GB1, B1 domain of the streptococcal immunoglobulin-binding protein G; TFE, 2,2,2-trifluoroethanol; bis-ANS, 1,1′-bis(4-anilinonaphthalene-5-sulfonic acid); NMR, nuclear magnetic resonance; TROSY-HSQC, transverse relaxation-optimized heteronuclear single-quantum coherence; DLS, dynamic light scattering; SEC, size exclusion chromatography; GWG, Gly-Trp-Gly tripeptide; R_H, hydrodynamic radius; R_G, radius of gyration; $[\theta]$, molar ellipticity (in 10^3 degrees square centimeters per decimole); ThT, thioflavin T; V_x, cross-flow; SEM, standard error of the mean; ϵ_{280}, extinction coefficient at 280 nm (mM^{-1} cm^{-1}); Ha, hamster; Mo, mouse; MD, molecular dynamics.

10.1021/bi800253c CCC: $40.75 © XXXX American Chemical Society

Published on Web 05/13/2008

PrP species and infectious prions via two separate processes, whereby at least prion formation is controlled by species-specific host factors. According to a recent report, adding more repeats also diminishes the neuroprotective function of PrP^C, which is currently its most likely physiological role (*11*).

Structural analyses of mammalian recPrP (residues 23−231) by nuclear magnetic resonance spectroscopy (NMR) have shown that it consists of two equal-sized domains: a flexible, mostly unfolded N-terminus (residues 23−120) and a globular, mostly α-helical C-terminus (residues 121−231) (*12*). The N-terminal tail contains a middle section of four consecutive eight-residue repeats [octarepeats (ORs)] flanked by a highly basic segment and a hydrophobic segment (residues 23−50 and 99−120, respectively). In human and hamster PrP, there are four perfect repeats (PHGGGWGQ; residues 60 and 91) with two imperfect repeats on either side: residues 51−59 (PQGGGTWGQ) and 92−98 (GGGTH-NQ; N97S in humans). The murine OR domain (MoOR) differs in two respects: the two central repeats are PHGGSWGQ, and the first partial repeat is PQGGTWGQ.

Despite their flexibility, the OR domain is probably not genuinely disordered, particularly at physiological pH (*13, 14*). According to circular dichroism (CD) spectra, OR conformations include a polyproline helix type II conformation (PPII), in which the backbone is restricted to a narrow range of dihedral angles (φ, ψ, and ω of −75°, 145°, and 180°, respectively) (*15–17*). Such a conformation is not easily detected by NMR, particularly in repeat sequences, because it does not involve intramolecular hydrogen bonds (*16*). The PPII far-UV CD signature consists of a negative peak near 200 nm and a positive one around 220 nm, whereby the latter is lower in intensity than the former. CD can conclusively distinguish between PPII and a disordered conformation via two diagnostic tests. First, the intensity of both peaks drops off reversibly with an increase in temperature, producing an isodichroic point at ∼210 nm (*18*). Second, the magnitude of the ∼220 nm peak increases in the presence of chaotropic agents such as urea or guanidinium-HCl (*19*).

A fluorescence resonance energy transfer (FRET) study in combination with molecular dynamics (MD) simulations has provided additonal evidence for the partial structuring of ORs in solution. When the effect of FRET between Trp residues (donor) and an N-terminally linked dansyl moiety (acceptor) was measured in several one- and two-OR peptides, the average interchromophore distance (Förster radius) was found to be 2−4-fold smaller than what had been expected from a fully extended peptide, as corroborated by MD simulations (*20*). It was proposed that this apparent compactness of the OR peptides was based on a cation−π interaction between the His and Trp side chains, a feature that had also been inferred from NMR data (*14*). Furthermore, a recent MD study of a two-OR peptide indicated that the GWGQ section regularly adopts a hydrogen-bonded bend- or turnlike conformation (*21*).

Previously, we demonstrated that wild-type (wt) and expOR domains have strikingly different ligand binding properties, using both hamster/human and mouse repeats (*22*). First, an expOR domain consisting of at least 10 consecutive repeats bound PrP^{Sc} but did so only at pH >7 and in the absence of copper and zinc, in a highly stable complex under denaturing conditions. Second, we found that expOR domains self-associated at pH >7, causing GST−expOR fusion proteins to multimerize in a highly distinctive manner. Multimerization, however, was found not to be a prerequisite for PrP^{Sc} binding.

Under physiological conditions, the ORs bind copper in at least three different metal occupancy modes, each with a particular inter- or intrarepeat copper coordination and backbone conformation (*23*). Currently, any direct connection between PrP's ability to bind copper and its physiological function remains to confirmed. Conversely, it is unclear how copper binding affects prion conversion (*24*). We showed that the wtOR domain binds PrP^C in the presence of either copper or zinc, while copper blocked binding of the expOR domain to PrP^{Sc} (*22*). This finding has since then been corroborated using OR peptides immobilized on micelles that mimic the physiological environment of PrP^C (*25*). An intitial model based on the findings mentioned above proposed that PrP-expOR could bind and stabilize short-lived PrP^{Sc}-like folding intermediates, thereby rescuing them from regular clearance in vivo. In addition, the mutant itself might more easily convert to PrP^{Sc}. Both events could take place within a homomeric PrP^C-expOR complex, possibly in an autocatalytic manner.

Here, we determined the effect of OR domain expansion on the folding behavior of isolated OR domains and full-length recMoPrP to determine why this type of mutation makes PrP more prone to spontaneous prion conversion.

MATERIALS AND METHODS

Materials. The HaPrP(55−67) and PrP(55−98) peptides were synthesized by the Biomedizinisches Forschungszentrum at the University of Düsseldorf (BMFZ). Sy-HaPrP(23−98) was isolated via thrombin digestion of the GST−PrP(23−98) fusion protein (*22*). The tripeptide H-Gly-Trp-Gly-OH (GWG) and glutaraldehyde were from Bachem AG and Sigma, respectively. NTA agarose was from Qiagen (Germany); all other purification media were from Amersham Biosciences.

Plasmids. The expression construct for wild-type MoPrP (pET-11a-MoPrP) has been described previously (*22*). pET-11a-MoPrP-14OR was made by replacing residues 53−94 (*Bsu*36I/*Kpn*I) with the corresponding 14-OR insert from murine PG14 cDNA (*9*). Truncated MoPrP(121−231) was cloned into a modified pET-15b vector in frame with an N-terminal hexahistidine tag with a thrombin cleavage site. Due to the inherent instability of the expOR open reading frame (ORF), we also isolated MoPrP-11OR as a cloning artifact. GB1-OR expression vectors were cloned into pET-22b at *Nde*I/*Eco*RI by inserting the GB1 ORF (T2Q/I6A double mutant) and linker (PGGPAGS) at *Nde*I/*Bam*HI, followed by a 3′ *Bam*HI/*Eco*RI fragment containing eight, ten and thirteen hamster ORs from pGEX-4T3-10OR (*22*). Again, cloning yielded an additional GB1-4OR clone. We also cloned GB1 fused to either wild-type MoPrP(52−98) (4MoOR) or the MoPrP(52−98)-14OR fragment (14MoOR). All constructs were confirmed by DNA sequencing.

Expression. All proteins were expressed at 37 °C in *Escherichia coli* BL21(λDE3) Rosetta (Novagen) in LB medium (with 5 mM L-arginine, 5 mM $MgSO_4$, 100 μg/mL carbenicillin, and 35 μg/mL chloramphenicol) or minimal medium (M9 salts, 0.4% glucose, and 1 g/L $^{15}NH_4Cl$ with

vitamins, trace elements, and antibiotics). Expression was induced at midlog phase with 1 mM isopropyl β-D-1-thiogalactopyranoside (IPTG) for 3 h.

Purification of GB1-OR Fusion Proteins. Cells were lysed in 50 mM Tris-HCl (pH 8), 5 mM EDTA, 1% Triton X-100, 2 mM phenylmethanesulfonyl fluoride (PMSF), and 0.25 mg/mL lysozyme, followed by DNaseI treatment (with 20 mM $MgCl_2$). The cleared lysate (30 min at 20000*g*) was first dialyzed to 20 mM Tris-HCl (pH 8) and 500 mM NaCl and then purified by affinity chromatography on Zn^{2+}-NTA agarose and IgG-Sepharose, using an imidazole and pH step gradient, respectively. Lysate containing GB1 alone was dialyzed to 20 mM Tris-HCl (pH 8) and 1 mM EDTA and cleaned on Q-Sepharose and IgG-Sepharose.

Purification of Full-Length MoPrP. After lysis, pellets were dissolved in 50 mM Tris-HCl (pH 8), 2 mM EDTA, 1% CHAPS, 8 M urea, and 10 mM dithiothreitol. Both wild-type and mutant MoPrP were purified using SP-Sepharose and Zn^{2+}-NTA agarose. Cleaned MoPrP (0.5 mg/mL) was refolded by dialysis from 20 mM MOPS (pH 8), 1 mM EDTA, and 6 M urea to 5 mM sodium acetate (pH 4.7) (1:100, 4 °C). Monomeric MoPrP was isolated on a HiLoad 26/60 Sephacryl 75 column in 20 mM Tris-acetate (pH 4) and 50 mM NaCl. We verified that disulfide bond formation was equally efficient in all protein batches, which showed that a trace of disulfide-linked dimer was invariably formed as a byproduct [nonreducing SDS−PAGE (data not shown)]. Furthermore, we confirmed that all nonmonomeric material could be denatured and refolded again with similar results, thus ruling out any covalent modifications that could obstruct folding.

Purification of Truncated His_6-MoPrP (121−231). The pellet after lysis was dissolved in 50 mM Tris-HCl (pH 8), 2 mM imidazole, 500 mM NaCl, 20 mM β-mercaptoethanol, and 6 M GuHCl and applied to Ni^{2+}-NTA agarose. The protein was refolded by washing with 20 mM Tris-HCl (pH 8), 10 mM imidazole, and 500 mM NaCl at room temperature. After elution (200 mM imidazole) and dialysis, the His tag was removed by thrombin digestion in 20 mM Tris-HCl (pH 8.3), 300 mM NaCl, and 1 mM EDTA (1 unit/mg for 90 min, room temperature). Monomers were isolated as described above.

CD Spectroscopy. Spectra were recorded on a Jasco J-815 instrument with a temperature controller, using either a 0.2 cm (far-UV) or 1.0 cm (near-UV) cuvette. Settings were as follows: 1 nm bandwidth, 50 nm/min scan, 2 s response time, 40 accumulations. Buffers were as follows: 10 mM sodium acetate at pH 4, 10 mM Tris-acetate at pH 8, 0.1 mM EDTA and 20 mM Tris-acetate at pH 4, and 50 mM NaCl. Melting curves (monitored at 222 nm) were averaged over three separate runs: 5 μM protein, from 25 to 85 °C at a rate of 1 °C/min. Curves were fitted using Jasco spectra analysis version 1.53. Spectra were normalized to molar ellipticity units ($[\theta]$ in 10^3 degrees square centimeters per decimole) per residue, Trp, or molecule. CDSSTR secondary structure estimates were performed at DICHROWEB (*26*). In each case, the normalized root-mean-square deviation (nrmsd) between experimental data and fitted curve was less than 0.04.

aFFFF. System: Eclipse 2 equipped with HELEOS, Optilab Rex (Wyatt Technologies), and a multiple-wavelength detector (Agilent). Software: Eclipse 2.5 and Astra 5.3.1.4. Conditions: MoPrP was separated in 20 mM Tris-acetate (pH 4) and 50 mM NaCl with a channel flow of 1 mL/min, using a 490 μm spacer and 5 kDa MWCO cellulose membrane. Flow scheme: sample inject (75 μL), focusing [2 min, 3 mL/min cross-flow (V_x)], first elution phase (25 min, 1.6 mL/min linear V_x), second phase (20 min, 1.6 to 0.15 mL/min V_x gradient), third phase (10 min V_x off). For GB1 and GB1-4/14MoOR, we set V_x to 2 mL/min. Extinction coefficients at 280 nm (±SEM) were determined from four separate runs using the 100% recovery method in Astra 5.3.1.4.

NMR Spectroscopy. We recorded $^1H-^{15}N$ transverse relaxation-optimized heteronuclear single-quantum coherence (TROSY-HSQC) spectra at 25 °C using a Varian Unity INOVA 600 MHz spectrometer equipped with a Cold Probe. Scan settings for PrP were as follows: 32 transients over 680 (^1H) × 96 (^{15}N) complex points with spectral widths of 8000 (^1H) and 2500 Hz (^{15}N). For GB1: 24 scans over 680 (^1H) × 128 (^{15}N) complex points. Samples: 0.3−0.7 mM ^{15}N-labeled protein in 20 mM Tris-acetate (pH 4), 50 mM NaCl, 10 mM sodium azide, and 10% D_2O or 50 μM protein in 20 mM Tris-acetate (pH 8), 0.5 mM EDTA, 5 mM sodium azide, and 10% D_2O. Spectra were processed with NMRPipe and CARA (*27, 28*).

Fluorescence Spectroscopy. Spectra (20 accumulations each) were recorded on a Perkin-Elmer LS-50B spectrometer. In the ThT assay, 10 μM protein was preincubated with 10 μM ThT in 50 mM bis-Tris-acetate (pH 6.5) and 1 mM EDTA (30 min, room temperature). For emission, $\lambda_{exc} = 460$ nm and the emission and excitation slit widths were 5 nm. For excitation, $\lambda_{em} = 485$ nm, idem. For the bis-ANS assay, 0.25 μM monomer was preincubated with 1 μM bis-ANS in either 20 mM sodium acetate (pH 4) or 10 mM Tris-acetate (pH 8) and 0.1 mM EDTA. $\lambda_{exc} = 400$ nm, with emission and excitation slit widths of 4 nm.

Mass Spectrometry. All three full-length MoPrP proteins were analyzed by electron spray ionization time-of-flight mass spectrometry (ESI-TOF; by G. Sajnani, University of Santiago de Compostela, Santiago de Compostela, Spain), yielding values of 23148.96 Da for the wild type, 27929.81 Da for MoPrP-11OR, and 30320.54 Da for MoPrP-14OR. All are within 2 Da of the calculated value (Table 1).

Cross-Linking. MoPrP (0.5 mg/mL) was reacted with 20 mM glutaraldehyde in 25 mM sodium acetate (pH 5.2) with continuous shaking at 25 °C. The reaction was stopped by adding sample buffer; samples were run on 15% reducing SDS−PAGE gels.

Dynamic Light Scattering. Scattering profiles were recorded in a 3 mm cuvette on a DynaPro MS/X instrument (Wyatt Technologies) equipped with a temperature controller. Samples were measured in all buffers used for CD and aFFFF, at 50−500 μM protein depending on particle size. Data were analyzed using DYNAMICS V6. All R_H values are averages (±SEM) based on at least four separate data sets of ten measurements each.

Determination of Protein Concentrations. Protein concentrations were measured at 280 nm in 20 mM Tris-acetate (pH 4.0) and 50 mM NaCl. The ϵ_{280} values are listed in Table 1.

Prion Bioassay. Thirty microliters (of 1 μg/μL corresponding to ~1 nmol) of freshly refolded, noncentrifuged wild-type or mutant MoPrP (14OR) dialyzed to PBS was

Table 1: Overview of Protein and Peptide Constructs (wt, wild-type; exp, expanded) with Their Theoretical Molecular Masses (kilodaltons) and Experimentally Determined (by aFFFF) Extinction Coefficients at 280 nm (ϵ_{280} in mM^{-1} cm^{-1} ± SEM)[a]

description	molecular mass (kDa)	ϵ_{280} (mM^{-1} cm^{-1})
Gly-Trp-Gly (GWG)	0.32	4.6 ± 0.3
HaPrP(55−98) (OR-only peptide)	4.3	22.5
HaPrP(23−98) (plus Gly-Ser on N-terminus)	7.7	31.0
protein G B1 domain (GB1) with C-terminal linker (PGGPAGS)	6.7	10.3 ± 0.3
GB1-4OR (hamster/human wtOR domain)	9.8	28.3
GB1-4MoOR (murine wtOR domain, residues 52−98)	11.0	33.9 ± 0.6
GB1-10OR (hamster/human expOR domain; plus six ORs)	14.5	55.3
GB1-14MoOR (murine expOR domain; residues 52−98 plus nine ORs)	18.3	73.9 ± 1.8
truncated MoPrP(121−231) (plus Gly-Ser on the N-terminus)	13.3	19.8 ± 0.2
full-length wild-type MoPrP(23−231)	23.1	53.4 ± 1.0
full-length MoPrP(23−231)-11OR (plus seven ORs)	27.9	81.8 ± 1.7
full-length MoPrP(23−231)-14OR (plus nine ORs)	30.3	94.3 ± 1.2

[a] GB1-4OR and GB1-10OR had poor aFFFF profiles, and their ϵ_{280} values were calculated using 4.5 mM^{-1} cm^{-1} per OR. The same applied to the peptides, whereby that of GWG was determined by dry mass. The ϵ_{280} of HaPrP(23−98) included the theoretical PrP(23−54) value.

injected intracerabrally into young tga20 mice (*29*), with 10 animals per group (first passage). All mice were culled after 560 days, and three brains from each group were pooled and 20 μL of a 10% homogenate inoculated intracerebrally for the second passage (again 10 mice each). The two diseased mice in the mutant group were then passaged a third time to confirm infectivity, alongside controls from the wild-type group. Animals were examined daily for standard neurological symptoms and sacrificed according to animal protection regulations when severe clinical symptoms were observed. The animal experimentation protocol had been approved for L.S.

RESULTS

OR Conformers Have PPII and β-Turn Conformation. A previous CD-based study has provided strong evidence for PPII-like behavior of wild-type OR peptides (*17*). Here, we first wanted to confirm this observation and then compare it directly with that of expOR domains. To begin with, we characterized two N-terminal fragments of hamster (Ha) PrP by far-UV CD: PrP(55−98) (OR-only peptide) and PrP(23−98). Their far-UV CD spectra indeed matched the general PPII signature, showing both a negative peak and a positive peak at 198 and ∼224 nm, respectively (Figure 1A). In addition, each spectrum displayed PPII-like temperature (4−50 °C) and urea (6 M, at 4 °C) effects (Figure 1B). Likewise, the difference spectrum of PrP(55−98) versus PrP(23−98) showed similar but less pronounced effects, indicating that the basic PrP(23−50) segment has partial PPII-like character (Figure 1A of the Supporting Information) (*15*). However, we did not observe an isodichroic point for the PrP(55−98) peptide between 4 and 50 °C: the positive peak nearly completely disappeared, but the negative peak hardly changed. Recording spectra at pH 4 or 8 made little difference (Figure 1A). Apparently, the ORs do not undergo a simple two-state unfolding from PPII to disordered and must therefore contain additional conformers. By recording spectra in 70% trifluoroethanol (TFE), which generally stabilizes structures based on intrapeptide hydrogen bonds, we determined that ORs can also adopt a β-turn-like conformation (Figure 1B of the Supporting Information). Two turn-like OR conformers have in fact been described previously (*13, 14*).

The 2-fold enhancement of the 224 nm peak in the PrP(55−98) spectrum by urea is a strong indicator for high PPII content. Indeed, if we assume that the peptide is fully unfolded at 50 °C, up to half its residues are predicted to be in a PPII-like conformation at 4 °C (*30*). However, the presence of a tryptophan in each repeat makes accurate quantification impossible, because the Trp residues could give rise to inter-repeat exciton coupling, provided their indole side chains have a stable coplanar orientation and are separated by less than 1.5 nm. Such an effect can occur in ordered peptides and produce a strong PPII-like CD signal (*31*). To determine the minimal Trp contribution, we looked at the spectrum of a single tryptophan in the nonfolded tripeptide Gly-Trp-Gly (GWG). The GWG and OR spectra had similar peaks at 224 nm (Figure 1a), but the magnitude of the GWG peak was reduced by ∼25% in 6 M urea and also at 50 °C (data not shown). We therefore conclude that the PrP(55−98) spectrum does contain a Trp contribution but also that the OR conformers determine its magnitude, since the GWG-only signal cannot account for the temperature and urea effects in the OR spectum.

Inserting Extra Repeats Has Little Effect on the Isolated OR Domain. We originally employed GST-OR fusion proteins, because the OR fragments themselves are poorly soluble at physiological pH, however, because GST (glutathione *S*-transferase; 26 kDa) itself can form dimers, we switched to the thermostable and monomeric protein G B1 domain (GB1, 6 kDa). Here, we used 10OR and 14MoOR fragments as representatives of expOR domains, 10 repeats being the minimum for PrP^{Sc} binding (Table 1). Both constructs behaved essentially the same, unless mentioned specifically. All GB1-OR fusion proteins were expressed in soluble form in *E. coli* (Figure 2 of the Supporting Information). GB1 and GB1-wtOR were essentially monomeric under all conditions tested (up to 37 °C), having hydrodynamic radii (R_H) of 1.4 ± 0.2 nm (7 ± 2 kDa) and 1.9 ± 0.3 nm (15 ± 5 kDa), respectively. GB1-expOR was monomeric at pH 4 but multimeric at pH 8 with an R_H of 8.1 ± 0.5 nm (450 ± 70 kDa) at 25 °C. Above 30 °C, however, GB1-10OR reversibly dissociated into monomers, whereas the GB1-14MoOR multimers remained intact.

Subsequently, we verified by NMR spectroscopy that GB1 retains its overall fold in GB1-OR fusion proteins. We could identify at least 38 resonances in the $^1H-^{15}N$ TROSY-HSQC spectrum of GB1-wtOR belonging to residues that are part of secondary structure elements in the GB1 moiety (Figure 3A,B of the Supporting Information) (*32, 33*). Attachment of the wtOR fragment had a minor effect on these core residues, but it did affect the ones in the direct vicinity of the linkage site. Furthermore, the spectra of GB1-wtOR and GB1-expOR were closely overlapping, showing little to no dispersion of the Gly, His, Ser, Gln, and Trp resonances of the ORs (Figure 3C of the Supporting Information). On the basis of

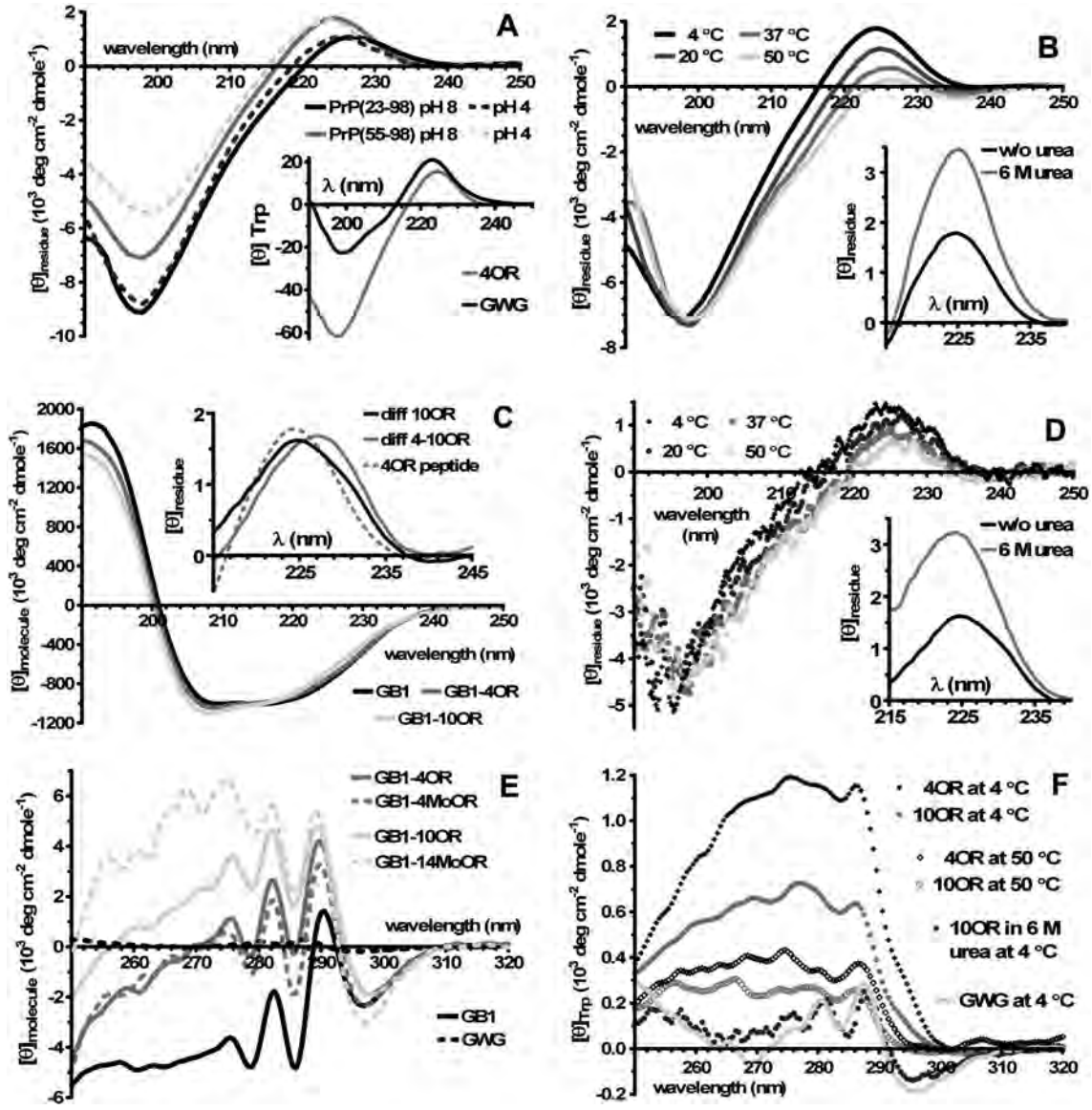

FIGURE 1: Far- and near-UV CD spectra of OR peptides and GB1-OR fusion proteins. To facilitate comparison, CD units are in molar ellipticity ($[\theta]$ in 10^3 degrees square centimeters per decimole) per residue, tryptophan, or molecule. (A) Far-UV spectra of HaPrP(55−98) and HaPrP(23−98) at pH 4 and 8, all at 4 °C. The inset compares GWG to HaPrP(55−98) in water (4OR). (B) Melting behavior of HaPrP(55−98) at pH 8, showing spectra at 4, 20, 37, and 50 °C. The inset shows the 224 nm peak with or without 6 M urea at pH 8 (4 °C). (C) Comparison of far-UV spectra of GB1, GB1-4OR, and GB1-10OR at pH 8 and 4 °C, illustrating their small spectral differences. The inset shows the close overlap between the 224 nm peaks of PrP(55−98) and the difference spectra of GB1 vs GB1-10OR and GB1-4OR vs GB1-10OR. (D) Temperature effect on the GB1 vs GB1-10OR difference spectrum like in panel B. (E) Near-UV CD spectra of GWG, GB1, GB1-4OR, GB1-4MoOR, GB1-10OR, and GB1-14MoOR at pH 4 and 4 °C. (F) Near-UV CD difference spectra of GB1 vs GB1-4OR and -10OR at 4 and 50 °C. The spectrum of GWG is shown again to demonstrate the effect of 6 M urea on the spectrum of the 10OR moiety; adding 70% TFE produced the same result.

these results, we conclude that the conformation of GB1 is sufficiently stable for us to determine the spectroscopic fingerprint of the expOR domain, albeit primarily in a qualitative manner.

The spectra of GB1 and the GB1-OR fusion proteins had a small yet significant spectral difference, having verified that the CD spectrum of GB1 itself was stable in the ranges of pH 4−8 and 4−50 °C (≤10% wavelength-independent intensity difference) (Figure 1C). Bearing that in mind, we found that the difference spectra of GB1-expOR versus GB1 and GB1-wtOR, meaning the CD profile of the expOR domain as a whole and that of the extra repeats, were comparable to that of the PrP(55−98) peptide (Figure 1D and Figure 1B of the Supporting Information). Varying the pH did not significantly affect the expOR spectrum (data not shown). Therefore, we conclude that insertion of extra repeats has little effect on the conformation of the isolated OR domain.

OR Conformers Display Trp-Related Ordering. The near-UV CD difference spectra of GB1, GB1-wtOR, and GB1-expOR offer a qualitative measure of the level of conformational freedom of the Trp indole side chains within each OR (*34*). At pH 4, both the wtOR and expOR fragments produced a temperature-dependent near-UV CD signal, namely a broad positive band between 250 and 300 nm that clearly differed from the GWG spectrum (Figure 1E,F). The wtOR moiety was more ordered per repeat than the expOR fragment, having an ∼40% higher signal. Switching to pH

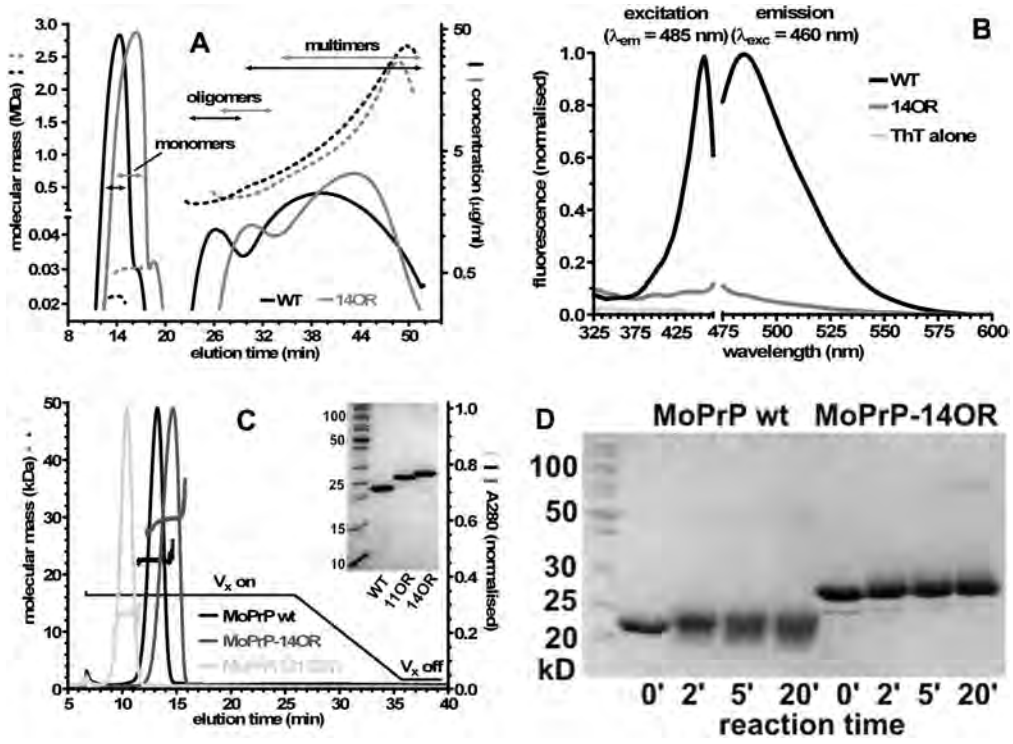

FIGURE 2: Refolding of wild-type (WT) and mutant recMoPrP (14OR). (A) aFFFF profile [elution vs both molar mass and concentration (micrograms per milliliter)] of refolded MoPrP after ultracentrifugation (100000*g*), showing monomers, soluble oligomers, and multimers. (B) Thioflavin T (ThT) excitation and emission fluorescence spectra of refolded MoPrP prior to centrifugation. (C) aFFFF profile (elution vs molar mass and 280 nm absorbance) of isolated monomers, including truncated MoPrP(121−231). The cross-flow (V_x) gradient (same as in panel A) shows the absence of both dimers and larger species. The inset (15% reducing SDS−PAGE) shows purified wild-type MoPrP (WT), MoPrP-11OR, and MoPrP-14OR to illustrate that recMoPrP-expOR has a stable number of repeats. (D) Cross-linking of wild-type MoPrP and MoPrP-14OR at pH 5.2 with glutaraldehyde for up to 20 min at room temperature (10% reducing SDS−PAGE).

8 lowered the overall intensity of both difference spectra by 30−40% (data not shown). The near-UV CD sginal was completely lost, meaning it became nearly identical to that of GWG, in both 6 M urea and 70% TFE, indicating that the Trp ordering is determined by a conformation other than PPII or β-turn.

Repeat Insertion Changes the Misfolding of Full-Length MoPrP. Having characterized isolated OR conformers, we then compared the wild type to mutant MoPrP(23−231) carrying seven or nine extra repeats (11OR or 14OR, respectively), using truncated MoPrP(121−231) for comparison (Table 1). The correct number of repeats in the full-length proteins was verified by mass spectrometry. Both MoPrP-expOR constructs yielded basically the same results, unless otherwise stated specifically. All three full-length proteins were exclusively expressed as inclusion bodies but could be refolded by dialysis in a reproducible manner. We then analyzed the refolding mixture to determine whether wild-type and mutant MoPrP differed in their ability to fold into native monomers or misfold into aggregates and/or amyloid.

Using asymmetric flow field-flow fractionation (aFFFF), we found that each protein yielded approximately equal amounts of monomers (20−25%, w/w, of total), soluble oligomers (~250−600 kDa, ~2%), soluble multimers (up to 2.5 MDa, ~8%), and insoluble aggregates (>10 MDa, 65−75%) (Figure 2A). The latter could be removed by ultracentrifugation (100000*g*, 1 h). CD analysis showed that all species of ≥250 kDa contained misfolded, β-sheet-rich protein (Figure 4 of the Supporting Information). Furthermore, we found that the aggregates of wild-type MoPrP contained at least 20 times more amyloid than the mutants, as determined by a thioflavin T (ThT) fluorescence assay (Figure 2B).

Closer inspection of aFFFF profiles showed that wild-type and mutant MoPrP (14OR) differed in the distribution of their soluble oligo- and multimers, even though their peaks roughly reflected the difference in monomer size: oligomers peaked at ~280 and 370 kDa, the multimers at ~1.0 and 1.3 MDa, respectively (Figure 2D). However, we saw that along the whole fractionation range the mutant complexes consistently had a lower molar mass than the wild-type ones eluting at that point, a feature that was found to be reproducible in several protein batches. We noticed moderately increased steric elution for the mutant due to its longer tail, causing some of the protein to elute faster. However, such an effect would actually shrink the difference between wild-type and mutant oligo- and multimers. Hence, the most likely explanation for this discrepancy is a (minor) difference in shape. Unfortunately, the intermediate aggregate fraction was too heterogeneous to generate a useful conformation plot, i.e., molar mass versus radius of gyration (R_G). Such a plot would quantiy the correlation between particle shape and molar mass, but on average, the oligomers had an R_G of >5 nm while multimers of >800 kDa had an R_G of 13.4 ± 0.5 nm. These figures were compatible with our DLS analysis, which also hinted at a distribution difference between the wild type and mutant, although we could not distinguish between mono- and oligomers. Following ultracentrifugation, refolded wild-type and mutant MoPrP both had two-state

scattering profiles with R_H values of 4.4 ± 1.5 nm (ca. 40−200 kDa) and 15.4 ± 2.3 nm (1.4−2.8 MDa) compared to 3.3 ± 1.0 nm (ca. 25−100 kDa) and 13.5 ± 2.5 nm (0.9−2.2 MDa), respectively.

MoPrP-expOR Does Not Multimerize Like the Corresponding GB1-OR Fusion Proteins. Full-length recPrP, especially PrP-expOR, is poorly soluble at pH >7. However, we noticed that its solubility depended strongly on the type and concentration of anions in solution, particularly chloride. In chloride-free Tris-acetate buffer (pH 8), the mutants were sufficiently soluble (∼30 μM) for DLS analysis. At pH 8, the 14OR mutant existed as small oligomers (R_H of ∼6 nm or ∼230 kDa) that readily dissociated above 30 °C. In contrast, both the wild type and 11OR mutant were probably monomeric (R_H ∼ 3 nm or 40 kDa). At pH 4, the wild type and both mutants had R_H values of 2.7 ± 0.3 nm (35 ± 10 kDa) and 3.2 ± 0.2 nm (50 ± 10 kDa), respectively. In comparison, all GB1-OR fusion proteins had a GB1-like scattering profile at pH 4 (R_H of 1.6 ± 0.5 nm or 11 ± 7 kDa), suggesting that their OR tails were fully extended and thus contributed little to overall scattering. Since MoPrP(121−231) had an R_H of 1.6 ± 0.3 nm (12 ± 3 kDa), irrespective of pH, the comparatively high R_H values of full-length MoPrP, in particular of the mutants, could be indicative of one of three things: (i) a monomer−dimer equilibrium, (ii) intramolecular binding between the N- and C-termini, or (iii) a relatively compact N-terminus. To distinguish between these possibilities, we performed aFFFF and covalent cross-linking experiments.

According to aFFFF analysis at pH 4, MoPrP-expOR did not form stable dimers but was monomeric like wild-type and truncated MoPrP (Figure 2A). The same applied to GB1, GB1-4MoOR, and GB1-14MoOR; GB1-4OR and -10OR had poor aFFFF profiles (data not shown). The molecular mass of each monomer was within 5% of the expected value (Table 1), calculated using the differential refractive index as a measure of protein concentration plus light scattering data (both measured in-line). By combining refractive index and UV absorbance, we could then deduce the respective extinction coefficients at 280 nm (ϵ_{280} in mM^{-1} cm^{-1}). To our surprise, we found that the measured ϵ_{280} values (Table 1) were significantly lower (by 16−18%) than the calculated ones (*35*). These data correspond to an ϵ_{280} per OR of approximately 4.5, compared to a "standard" ϵ_{280} for Trp of 5.5−5.6 (*35*). We also arrived at a value of 4.6 ± 0.3 when we determined the ϵ_{280} of the GWG peptide by dry weight. In comparison the ϵ_{280} values that we determined for MoPrP(121−231) and GB1 were within experimental error of the published value (*36*) and the calculated value, respectively. Therefore, we conclude that the aFFFF-derived ϵ_{280} values of full-length MoPrP represent a genuine correction, allowing us to determine accurate CD difference spectra of wild-type, mutant, and truncated MoPrP (see below).

Finally, to rule out any transient dimerization of the mutants, we incubated MoPrP with glutaraldehyde (at pH 5.2), an amine-reactive bifunctional cross-linker. We did not observe any oligomeric species, apart from a minor dimer band that probably arose from random collisions (Figure 2D). However, the wild type but not the mutant monomer band quickly became smeared or "fuzzy". We attributed this effect to the formation of intramolecular linkages between Lys residues that are distant in the primary sequence, turning the polypeptide into a nonlinear chain. If so, the presence of extra repeats prevented such intramolecular interactions within full-length PrP. Taken together, these data indicate that the N-terminus of PrP is not extended but has a condensed conformation, which would be compatible with a PPII-like conformation (see below) (*37*). It is also in accordance with an, on average, compact OR fold determined by FRET (*20*).

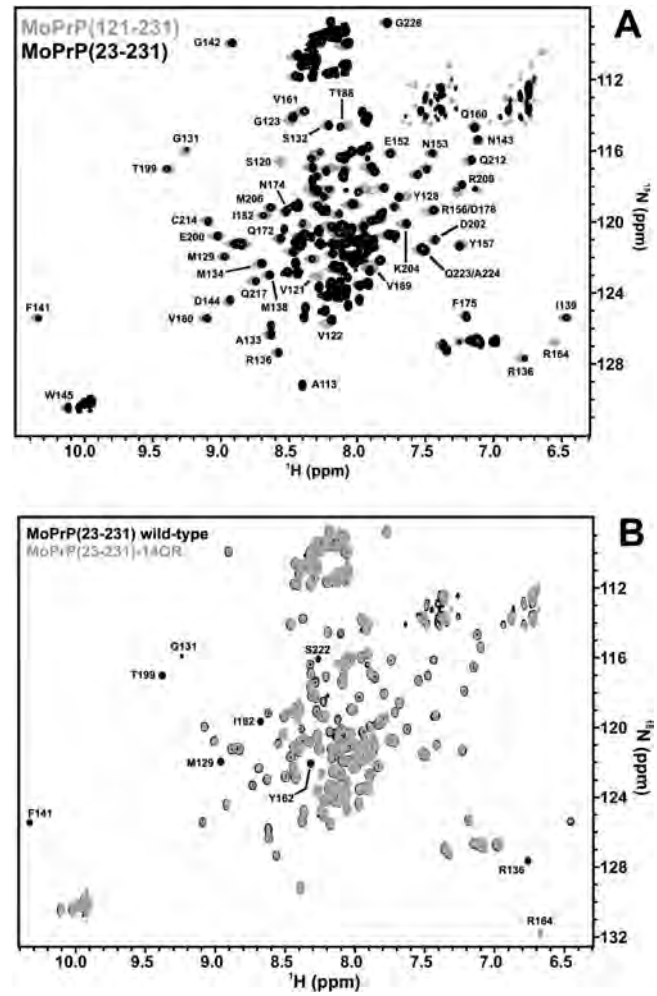

FIGURE 3: ^{1}H−^{15}N TROSY-HSQC NMR spectra (600 MHz) of truncated, wild-type, and mutant MoPrP in 20 mM Tris-acetate (pH 4) 50 mM NaCl, and 10% D_2O at 25 °C. (A) Annotated comparison of full-length and truncated MoPrP. The latter contains an N-terminal Gly119-Ser120 tail as a cloning artifact. (B) Comparison of wild-type MoPrP and MoPrP-14OR. Residues that exhibit a striking reduction in peak intensity in the mutant have been marked.

OR Expansion Does Not Affect Native Structure. To see whether the expOR domain had any effect on the conformation of the C-terminal domain, we recorded ^{1}H−^{15}N TROSY-HSQC NMR spectra of truncated, wild-type, and mutant MoPrP in aFFFF buffer (pH 4). Resonances were assigned on the basis of a reference spectrum of truncated MoPrP (Figure 3A) (*38*). Upon comparison of the spectra of wild-type and mutant MoPrP, all peaks were found to be overlapping with the exception of the side chain of Arg164 (Figure 3B). This residue seems to adopt two orientations in MoPrP that are characterized by ^{1}H−^{15}N resonances at 6.5 and 126.6 ppm (I) and 6.7 and 131.7 ppm (II), respectively. Orientation I is favored in the wild type and II

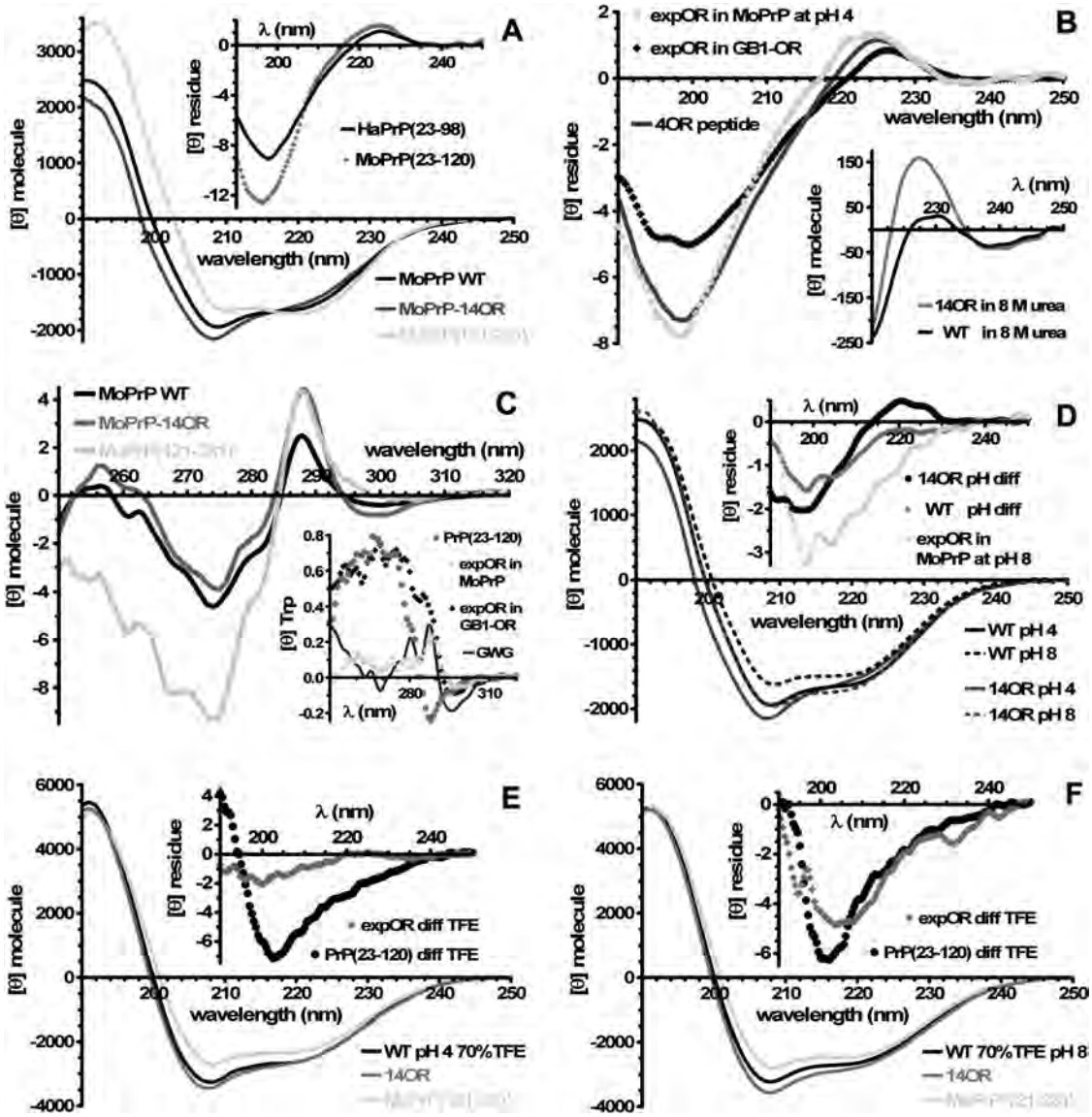

FIGURE 4: Far- and near-UV CD spectra of truncated, wild-type, and mutant MoPrP (14OR). (A) Far-UV spectra at pH 4 (4 °C). The inset shows the difference spectrum of truncated vs wild-type MoPrP [MoPrP(23−120) compared to HaPrP(23−98)]. (B) Difference spectra of panel A showing the wild type vs MoPrP-14OR (expOR in MoPrP at pH 4) compared to the difference spectrum of GB1-4MoOR vs GB1-14MoOR (expOR in GB1-OR fusion) and the HaPrP(55−98) peptide (4OR). The inset shows the effect of 8 M urea on the 224 nm peak of the wild type (WT) and MoPrP-14OR. (C) Near-UV spectra at pH 4 (4 °C). The inset shows the same difference spectra as in panel B but compared to GWG and the difference spectrum of full-length vs truncated MoPrP [PrP(23−120)]. (D) Far-UV spectra of wild-type and mutant MoPrP at pH 4 and 8 (20 °C). The inset shows the wild-type vs mutant difference spectrum at pH 8 (expOR in MoPrP at pH 8) plus the pH-induced spectral differences (pH diff) for each protein. (E) Same as in panel A but with 70% TFE at 20 °C. The inset shows the TFE difference spectra of the wild type vs truncated [PrP(23−120) diff TFE] and the wild type vs mutant (expOR diff TFE). (F) Same as in panel E but in 10 mM Tris-acetate at pH 8 and 20 °C. A structure estimate of the TFE difference spectra (both pH 4 and 8) illustrates that TFE stabilizes a β-like conformation of the N-terminus: ∼3% α-helix, ∼32% β-strand, ∼17% β-turn, and ∼48% disordered (all ±2%). TFE had largely the same effect per residue on the wild type and MoPrP-14OR, but the latter produced a higher β-shift at pH 8.

in the mutant. Furthermore, a specific set of resonances had a markedly lower intensity in mutant MoPrP, namely Met129, Gly131, Arg136 (side chain), Phe141, Tyr162, Thr199, and Ser222. However, we observed the same effect, albeit less pronounced, at these sites and also for the Arg164 side chain when we compared truncated to wild-type MoPrP (Figure 3A). Consequently, we conclude that insertion of repeats has essentially no effect on the conformation of the globular domain in PrP monomers at pH 4 but that the presence and length of the N-terminal tail may well modulate the dynamics of a select number of C-terminal residues.

The Expanded OR Domain Is PPII-like in Full-Length MoPrP at Low pH. Knowing that the C-terminus is a stable part of the overall conformation, we used far- and near-UV difference CD spectra of truncated, wild-type, and mutant MoPrP to determine the effect of repeat insertion on the N-terminus itself. At pH 4, the far-UV CD profile of the additional ORs was nearly identical to that of the PrP(55−98) peptide and comparable to that of the expOR moiety in GB1-14MoOR (Figure 4A,B). In contrast, the near-UV spectra showed that the Trp side chains were fully disordered in the extra repeats (Figure 4C). Furthermore, we observed that the spectrum of the wild-type N-terminus, i.e., the difference

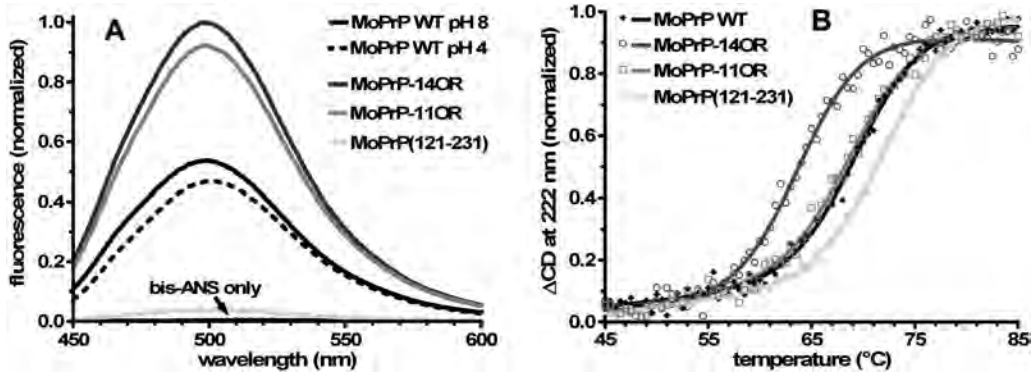

FIGURE 5: (A) Fluorescence spectra of bis-ANS bound to wild-type MoPrP at pH 4 and 8, compared to that of truncated MoPrP, MoPrP-11OR, and MoPrP-14OR at pH 8. (B) CD melting curves (222 nm) of truncated expOR, wild-type expOR, and both expOR mutants at pH 8.

between wild-type and truncated MoPrP, was similar to that of HaPrP(23−98) (Figure 4A). The presence of the PrP(99−120) segment added a negative peak at ∼198 nm, suggesting that it was mainly unfolded.

CD melting curves showed that the proteins differed little in their thermal stability at low pH. In aFFFF buffer, wild-type and truncated MoPrP both had a melting temperature (T_m) of 63.1 ± 0.5 °C, while MoPrP-expOR had a T_m of 62.3 ± 0.3 °C. In cross-linking buffer, however, all proteins had a T_m of 70 ± 0.4 °C. Moreover, all proteins had comparable hydrophobic exposure at pH 4, as determined by titration with 1,1′-bis(4-anilinonaphthalene-5-sulfonic acid) [bis-ANS (Figure 5A)], a well-established fluorescent reporter molecule for protein hydrophobicity.

The Conformation of the N-Terminus of MoPrP Shifts from PPII- to β-like at pH 8. Increasing the pH from 4 to 8 had a significant effect on the CD spectrum of wild-type MoPrP, whereas that of truncated MoPrP(121−231) was not affected (Figure 4D). According to a structure estimate (CDSSTR), wild type MoPrP underwent the following α-to-β conformational shift: 20 to 17% α-helix, 25 to 30% β-strand, 35 to 31% disordered, with β-turns remaining constant at 20%. The same analysis of truncated MoPrP yielded 46% α-helix, 19% β-strand, 18% β-turn, and 17% disordered. In comparison, the NMR structure has 48% α-helix, 4% β-strand, 11% turn, and ∼38% loop residues in the NMR structure (*38*). Hence, this method appears to give a good estimate of the α-helical content of the globular domain. We presume that the large amount of predicted β-structure stems from the fact that the loop residues are conformationally constrained (*12*), causing their net CD signature to be more β-like than random coil. As a result, we conclude that the full-length protein has fewer helical residues at high pH but that the apparent increase in the β-structure level mainly reflects overall ordering of the N-terminus, in accordance with earlier NMR data (*13*). The $^1H-^{15}N$ TROSY-HSQC spectra of both proteins were indeed very similar at pH 8, indicating that the stably hydrogen bonded residues in the globular domain are not involved in any conformational rearrangement (Figure 5 of the Supporting Information). Likewise, human PrP(121−230) was found to have the same basic fold at low and neutral pH (*39*).

We subsequently tested whether TFE could mimic the structuring effect of pH on the N-terminus. The difference spectra of wild-type and truncated MoPrP in 70% TFE showed that the N-terminus was stabilized as a β-like conformer (Figure 4E,F). TFE had a markedly different effect on the N-terminus in MoPrP than on the HaPrP(55−98) or HaPrP(23−98) peptides (Figure 1B of the Supporting Information), suggesting that the hydrophobic segment plays an essential part in the conformational shift. We, however, failed to observe a clear pH effect, which could mean that low pH overrides the intrinsic propensity of the N-terminus for a β-like conformation. Instead, a PPII-like conformation is favored at pH 4.

OR Expansion Changes the pH Response of the N-Terminus. The upward pH shift had a distinct effect on the CD spectrum of MoPrP-expOR, one that differed significantly from what we saw for the wild-type protein (Figure 4D). The difference spectrum between the wild type and mutant at pH 8 exhibited a broad negative band instead of a PPII-like curve (compare panels B and D of Figure 4). The distinction was further illustrated by the pH 4 to 8 difference spectrum of the mutant itself, which also did not match the wild-type one (Figure 4D). For MoPrP-14OR, the CDSSTR estimates at pH 4 and 8 differed by ≤2%, while all but the β-strand values had the opposite sign in comparison to that of the wild type: 8 to 9% α-helix, 33 to 34% β-strand, 19 to 21% turn, and 39 to 37% disordered. Furthermore, MoPrP-14OR had a higher β-preference than the wild type in TFE at pH 8 (Figure 4E,F). MoPrP-11OR yielded comparable results, which means that the oligomerization is not a factor here. So far, we have been unable to obtain useful $^1H-^{15}N$ TROSY-HSQC spectra of the mutants at pH 8.

The differential effect of pH on MoPrP-expOR was corroborated by bis-ANS binding (Figure 5A). Both mutants but not the wild type produced an ∼40% higher fluorescence at pH 8. Under these conditions, the hydrophobic binding area on PrP resides mainly in the N-terminus, because truncated MoPrP(121−231) bound hardly any bis-ANS. The latter effect probably reflects a (minor) change in tertiary structure, judging from the pH-dependent shift in its near-UV spectrum (Figure 6A,B of the Supporting Information). We also found that the T_m of MoPrP-14OR was significantly lower at pH 8 than for both wild-type MoPrP and MoPrP-11OR, namely, 63.9 ± 0.4 °C versus 69.7 ± 0.2 and 69.0 ± 0.2 °C, respectively (Figure 4G). Again, the difference between the two mutants cannot result from oligomerization since MoPrP-14OR is monomeric at >30 °C. In comparison, truncated MoPrP(121−231) had a T_m of 72 ± 0.2 °C, indicating that the N-terminus lowers the stability of full-length PrP.

Recombinant MoPrP-expOR Contains Prion Infectivity. To test whether any of the effects of OR domain expansion mentioned above caused recMoPrP to become neurotoxic and/or infectious, we injected wild-type and mutant (14OR) protein intracerebrally into MoPrP-overexpressing tga20 mice (first passage) (*29*). Here, we did not observe any adverse effects (acute or delayed). After almost 2 years, we intracerebrally inoculated the pooled brain homogenate from three animals of each group into new mice (second passage). Now, two mice in the mutant MoPrP group became ill after 137 and 140 days with characteristic symptoms and PrP^{Sc} deposition. In contrast, the wild-type MoPrP inoculated group remained symptom-free (> 500 days). To confirm infectivity, brain homogenates from the sick animals and healthy controls from the second passage were passaged a third time, whereupon all animals in the mutant group quickly developed disease (60 ± 2 days), whereas none of the controls did.

DISCUSSION

In this paper, we have looked at the folding behavior of full-length MoPrP with or without an expOR domain, using aFFFF analysis, ThT staining, and NMR and CD spectroscopy. First of all, we found that the expOR domain had basically no effect on the folding efficiency of α-helical, native monomers. However, we did find a profound effect on the misfolding pathway of PrP. Under the conditions used here, the presence of extra ORs strongly inhibited the formation of PrP amyloid. We also saw a small but distinct effect on the shape of soluble, β-rich oligo- and multimers. Moreover, we detected significant pH-dependent conformational differences between wild-type and mutant monomers. We therefore propose that the way in which MoPrP-expOR misfolds in vitro reflects major aspects of the pathogenic mechanism of PrP^{C}-expOR. Our finding that mutant but not wild-type MoPrP induced prion disease in some tga20 mice supports this idea.

Apparently, recombinant MoPrP-expOR either contains a low titer of infectious prions or is able to induce conversion of host PrP^{C}, albeit with low efficiency. Either way, these data suggest that de novo prion infectivity can be generated using nonfibrillar, bacterially expressed MoPrP-expOR and be transmitted to mice that express wild-type MoPrP. A previous study has shown 100% transmission when truncated MoPrP(89−230) was injected in fibrillar form into mice expressing that same truncated construct (*3*). Taken together, these data suggest that the N-terminus is a critical regulator for de novo prion conversion of full-length PrP^{C} in vivo.

There is a growing body of evidence which shows that aggregate species other than the "classical" protease resistant PrP^{Sc} can be neurotoxic or infectious (*40, 41*). The $MoPrP^{C}$-14OR that accumulated in neuronal aggregates in Tg(PG14) mice was in many ways PrP^{Sc}-like, but it was non-amyloidal and only weakly protease resistant (*8, 9*). In patients with OR insertions, specific testing of PrP-immunopositive neuronal plaques for amyloid (by Congo red) has only been reported for a limited number of cases, but a positive result does not appear to be a prerequisite for disease (*42*). Depending on the model system, there is an imperfect correlation between the presence and amount of fibrillar PrP^{Sc} and the prion titer of brain extracts (*43*). A better predictive measure for amyloid infectivity is probably fibril brittleness, meaning how easily different types of fibrils will fragment. In simple terms, the faster the breakup rate, the higher the prion titer (*44*).

Two recent studies have stated that the presence of an expOR domain actually accelerates fibril formation in vitro (*45, 46*). However, the study by Moore et al. used truncated hamster PrP(23−144) that is particularly amyloid prone, making it poorly comparable to our data (*45*). Dong et al. reported that substituting the N-terminal oligopeptide region of the yeast prion protein SUP35 with mammalian ORs made the chimeric protein more susceptible to fibrillization both in vitro and in yeast cells (*46*). Still, that report does not necessarily compare to neuronal prion conversion of full-length PrP in mammals, but it does show that the expOR domain is not an inherent obstacle to amyloid formation. Moreover, MoPrP-14OR aggregates from Tg(PG14) mice cannot seed prion conversion (*47*), something that SUP-expOR can do in yeast.

In our previous work, we suggested that the combination of homomeric binding between expOR domains and the capture of PrP^{Sc}, both of which are copper-independent but pH-dependent, might be the driving force behind de novo prion formation by PrP^{C}-expOR in vivo (*22*). Here, we investigated this idea further and found that homomeric binding also depends on temperature, breaking down above 30 °C. Furthermore, MoPrP-expOR proved to be much less amenable to self-association at pH >7 than GB1-expOR fusion proteins. Our findings suggest that the way in which PrP-expOR misfolds is the key event for prion genesis, whereas altered self-association may be just secondary to this.

In our view, there are three feasible and mutually complementary mechanisms that could explain the altered misfolding of MoPrP-expOR, including the near absence of amyloid. First, the soluble complexes of wild-type MoPrP but not those of the mutant are amyloid precursors due to subtle morphological differences between the two. This type of intermediate aggregate is of particular interest in regard to prion infectivity, because a recent aFFFF-based study has demonstrated that similar-sized PrP^{Sc} particles (620 ± 331 kDa; R_G of 12.1 ± 2.0 nm) have the highest infectivity per PrP content (*48*). Furthermore, $MoPrP^{C}$-14OR aggregates from transgenic mice had a sedimentation coefficient between 16 and 20 S, which is reportedly equivalent to 20−30 monomers (600−900 kDa) (*10*). If correct, the MoPrP-expOR oligo- and multimers, which are a byproduct in vitro, may in fact be the dominant species in vivo.

Second, spontaneous amyloid seeding is greatly reduced in MoPrP-expOR, because it has lost one or more intramolecular interactions that do occur in wild type MoPrP. Several NMR studies of full-length PrP have hinted at a transient interaction between N- and C-termini (*12, 49*). A recent study of HaPrP(90−231) dimers, based on carboxyl−amine cross-linking, identified inter- and intramolecular contacts between two segments, namely, residues 90−106 and 195−204 (*50*). Such an interaction could explain our cross-linking results, since both segments contain Lys residues that can react with glutaraldehyde. If confirmed, the loss of this interaction in MoPrP-expOR could be important to prion conversion, because any change in the dynamics of the PrP(90−106) region has the potential of influencing PrP^{Sc} formation (*51*).

Third, we found a distinct difference in conformation between wild-type and mutant PrP monomers, one that was most pronounced at pH 8. Judging from CD, bis-ANS fluorescence, and two-dimensional NMR data, that difference probably resides mainly in any or all of the three segments of the N-terminal tail. Such an initial difference in conformation may well cause wild-type and mutant PrP to enter different aggregation pathways once they have failed to enter the native folding route, taking into account that our refolding protocol includes a high-to-low pH gradient. An MD study of the aggregation dynamics of a chimeric polyglutamine protein, chymotrypsin inhibitor 2 carrying a loop with glutamine insertions (CI2-polyQ), hints at a mechanism that would integrate the latter two effects with our earlier findings (*22*). The presence of 4−10 glutamines causes CI2 to switch from exclusively monomeric to partially oligomeric, in a manner that involves nativelike domain swapping within the stably folded dimer rather than intermolecular interactions between the exogenous glutamines (*52*). An MD simulation, validated by the crystal structure of the CI2-4Q dimer, then showed how longer polyQ streches (up to 80 residues) could cause the chimera to aggregate when the glutamine interactions start to predominate over the oligomer contacts in the core domain, even though the intrinsic thermodynamic stability of CI2 remains unaffected (*53*). The calculated transition point nearly exactly matched the pathogenic threshold observed in mutant Huntingtin (∼35 Q). Likewise, self-association between expOR domains could interfere with the amyloid nucleation event of PrP, a process that may well depend on domain swapping (*54*), by increasing the lifetime of aggregation-prone folding intermediates that would otherwise quickly collapse via nativelike interactions. A recent modeling study of the C-terminal domain has put forward just such an intermediate (*55*). If so, that would mean that prion initiation is indeed fundamentally different from PrP amyloid formation.

ACKNOWLEDGMENT

We thank Dr. Gustavo Sajnani (University of Santiago de Compostela) for performing mass spectrometry analysis (MALDI and ESI-TOF) of full-length recPrP. We are also grateful to Dr. Simone Hornemann (ETH, Zürich, Switzerland) for supplying the $^{1}H-^{15}N$ chemical shift list of MoPrP(121−231).

SUPPORTING INFORMATION AVAILABLE

Additional CD and NMR data of PrP N-terminal peptides, GB1-OR fusion proteins, and MoPrP constructs in support of several key findings presented in this work is available. This material is available free of charge via the Internet at http://pubs.acs.org.

REFERENCES

1. Prusiner, S. B. (1998) Prions. *Proc. Natl. Acad. Sci. U.S.A. 95*, 13363–13383.
2. Safar, J. G., Kellings, K., Serban, A., Groth, D., Cleaver, J. E., Prusiner, S. B., and Riesner, D. (2005) Search for a prion-specific nucleic acid. *J. Virol. 79*, 10796–10806.
3. Legname, G., Baskakov, I. V., Nguyen, H. O., Riesner, D., Cohen, F. E., DeArmond, S. J., and Prusiner, S. B. (2004) Synthetic mammalian prions. *Science 305*, 673–676.
4. Kong, Q., Surewicz, W. K., Petersen, R. B., Zou, W., Chen, S. G., Gambetti, P., Parchi, P., Capellari, S., Goldfarb, L. G., Montagna, P., Lugaresi, E., Piccardo, P., and Ghetti, B. (2004) Inherited prion disease, in *Prion biology and diseases* (Prusiner, S. B., Ed.) 2nd ed., pp 673−775, Cold Spring Harbor Laboratory Press, Plainview, NY.
5. Brown, P., Gibbs, C. J., Jr., Rodgers-Johnson, P., Asher, D. M., Sulima, M. P., Bacote, A., Goldfarb, L. G., and Gajdusek, D. C. (1994) Human spongiform encephalopathy: The National Institutes of Health series of 300 cases of experimentally transmitted disease. *Ann. Neurol. 35*, 513–529.
6. Mead, S., Poulter, M., Beck, J., Webb, T. E., Campbell, T. A., Linehan, J. M., Desbruslais, M., Joiner, S., Wadsworth, J. D., King, A., Lantos, P., and Collinge, J. (2006) Inherited prion disease with six octapeptide repeat insertional mutation-molecular analysis of phenotypic heterogeneity. *Brain 129*, 2297–2317.
7. Goldfarb, L. G., Brown, P., McCombie, W. R., Goldgaber, D., Swergold, G. D., Wills, P. R., Cervenakova, L., Baron, H., Gibbs, C. J., Jr., and Gajdusek, D. C. (1991) Transmissible familial Creutzfeldt-Jakob disease associated with five, seven, and eight extra octapeptide coding repeats in the PRNP gene. *Proc. Natl. Acad. Sci. U.S.A. 88*, 10926–10930.
8. Castilla, J., Gutierrez-Adan, A., Brun, A., Pintado, B., Salguero, F. J., Parra, B., Segundo, F. D., Ramirez, M. A., Rabano, A., Cano, M. J., and Torres, J. M. (2005) Transgenic mice expressing bovine PrP with a four extra repeat octapeptide insert mutation show a spontaneous, non-transmissible, neurodegenerative disease and an expedited course of BSE infection. *FEBS Lett. 579*, 6237–6246.
9. Chiesa, R., Piccardo, P., Ghetti, B., and Harris, D. A. (1998) Neurological illness in transgenic mice expressing a prion protein with an insertional mutation. *Neuron 21*, 1339–1351.
10. Chiesa, R., Piccardo, P., Quaglio, E., Drisaldi, B., Si-Hoe, S. L., Takao, M., Ghetti, B., and Harris, D. A. (2003) Molecular distinction between pathogenic and infectious properties of the prion protein. *J. Virol. 77*, 7611–7622.
11. Li, A., Piccardo, P., Barmada, S. J., Ghetti, B., and Harris, D. A. (2007) Prion protein with an octapeptide insertion has impaired neuroprotective activity in transgenic mice. *EMBO J. 26*, 2777–2785.
12. Riek, R., Hornemann, S., Wider, G., Glockshuber, R., and Wuthrich, K. (1997) NMR characterization of the full-length recombinant murine prion protein, mPrP(23−231). *FEBS Lett. 413*, 282–288.
13. Zahn, R. (2003) The octapeptide repeats in mammalian prion protein constitute a pH-dependent folding and aggregation site. *J. Mol. Biol. 334*, 477–488.
14. Yoshida, H., Matsushima, N., Kumaki, Y., Nakata, M., and Hikichi, K. (2000) NMR studies of model peptides of PHGGGWGQ repeats within the N-terminus of prion proteins: A loop conformation with histidine and tryptophan in close proximity. *J. Biochem. 128*, 271–281.
15. Blanch, E. W., Gill, A. C., Rhie, A. G., Hope, J., Hecht, L., Nielsen, K., and Barron, L. D. (2004) Raman optical activity demonstrates poly(L-proline) II helix in the N-terminal region of the ovine prion protein: Implications for function and misfunction. *J. Mol. Biol. 343*, 467–476.
16. Bochicchio, B., and Tamburro, A. M. (2002) Polyproline II structure in proteins: Identification by chiroptical spectroscopies, stability, and functions. *Chirality 14*, 782–792.
17. Smith, C. J., Drake, A. F., Banfield, B. A., Bloomberg, G. B., Palmer, M. S., Clarke, A. R., and Collinge, J. (1997) Conformational properties of the prion octa-repeat and hydrophobic sequences. *FEBS Lett. 405*, 378–384.
18. Chellgren, B. W., Miller, A. F., and Creamer, T. P. (2006) Evidence for polyproline II helical structure in short polyglutamine tracts. *J. Mol. Biol. 361*, 362–371.
19. Whittington, S. J., Chellgren, B. W., Hermann, V. M., and Creamer, T. P. (2005) Urea promotes polyproline II helix formation: Implications for protein denatured states. *Biochemistry 44*, 6269–6275.
20. Gustiananda, M., Liggins, J. R., Cummins, P. L., and Gready, J. E. (2004) Conformation of prion protein repeat peptides probed by FRET measurements and molecular dynamics simulations. *Biophys. J. 86*, 2467–2483.
21. Pushie, M. J., and Vogel, H. J. (2007) Molecular dynamics simulations of two tandem octarepeats from the mammalian prion protein: Fully Cu^{2+}-bound and metal-free forms. *Biophys. J. 93*, 3762–3774.
22. Leliveld, S. R., Dame, R. T., Wuite, G. J., Stitz, L., and Korth, C. (2006) The expanded octarepeat domain selectively binds prions

and disrupts homomeric prion protein interactions. *J. Biol. Chem. 281*, 3268–3275.
23. Millhauser, G. L. (2007) Copper and the prion protein: Methods, structures, function, and disease. *Annu. Rev. Phys. Chem. 58*, 299–320.
24. Caughey, B., and Baron, G. S. (2006) Prions and their partners in crime. *Nature 443*, 803–810.
25. Kenward, A. G., Bartolotti, L. J., and Burns, C. S. (2007) Copper and zinc promote interactions between membrane-anchored peptides of the metal binding domain of the prion protein. *Biochemistry 46*, 4261–4271.
26. Lobley, A., Whitmore, L., and Wallace, B. A. (2002) DICHROWEB: An interactive website for the analysis of protein secondary structure from circular dichroism spectra. *Bioinformatics 18*, 211–212.
27. Keller, R. (2004) *The Computer Aided Resonance Assignment Tutorial* version 1.8.4, CANTINA Verlag, Goldau, Switzerland.
28. Delaglio, F., Grzesiek, S., Vuister, G. W., Zhu, G., Pfeifer, J., and Bax, A. (1995) NMRPipe: A multidimensional spectral processing system based on UNIX pipes. *J. Biomol. NMR 6*, 277–293.
29. Fischer, M., Rulicke, T., Raeber, A., Sailer, A., Moser, M., Oesch, B., Brandner, S., Aguzzi, A., and Weissmann, C. (1996) Prion protein (PrP) with amino-proximal deletions restoring susceptibility of PrP knockout mice to scrapie. *EMBO J. 15*, 1255–1264.
30. Kelly, M. A., Chellgren, B. W., Rucker, A. L., Troutman, J. M., Fried, M. G., Miller, A. F., and Creamer, T. P. (2001) Host-guest study of left-handed polyproline II helix formation. *Biochemistry 40*, 14376–14383.
31. Grishina, I. B., and Woody, R. W. (1994) Contributions of tryptophan side chains to the circular dichroism of globular proteins: Exciton couplets and coupled oscillators. *Faraday Discuss.,* 245–262.
32. Kuszewski, J., Clore, G. M., and Gronenborn, A. M. (1994) Fast folding of a prototypic polypeptide: The immunoglobulin binding domain of streptococcal protein G. *Protein Sci. 3*, 1945–1952.
33. Gronenborn, A. M., and Clore, G. M. (1996) Rapid screening for structural integrity of expressed proteins by heteronuclear NMR spectroscopy. *Protein Sci. 5*, 174–177.
34. Kelly, S. M., and Price, N. C. (2000) The use of circular dichroism in the investigation of protein structure and function. *Curr. Protein Pept. Sci. 1*, 349–384.
35. Pace, C. N., Vajdos, F., Fee, L., Grimsley, G., and Gray, T. (1995) How to measure and predict the molar absorption coefficient of a protein. *Protein Sci. 4*, 2411–2423.
36. Liemann, S., and Glockshuber, R. (1999) Influence of amino acid substitutions related to inherited human prion diseases on the thermodynamic stability of the cellular prion protein. *Biochemistry 38*, 3258–3267.
37. Zagrovic, B., Lipfert, J., Sorin, E. J., Millett, I. S., van Gunsteren, W. F., Doniach, S., and Pande, V. S. (2005) Unusual compactness of a polyproline type II structure. *Proc. Natl. Acad. Sci. U.S.A. 102*, 11698–11703.
38. Riek, R., Hornemann, S., Wider, G., Billeter, M., Glockshuber, R., and Wuthrich, K. (1996) NMR structure of the mouse prion protein domain PrP(121−321). *Nature 382*, 180–182.
39. Calzolai, L., and Zahn, R. (2003) Influence of pH on NMR structure and stability of the human prion protein globular domain. *J. Biol. Chem. 278*, 35592–35596.
40. Barron, R. M., Campbell, S. L., King, D., Bellon, A., Chapman, K. E., Williamson, R. A., and Manson, J. C. (2007) High titers of transmissible spongiform encephalopathy infectivity associated with extremely low levels of PrPSc in vivo. *J. Biol. Chem. 282*, 35878–35886.
41. Lasmezas, C. I., Deslys, J. P., Robain, O., Jaegly, A., Beringue, V., Peyrin, J. M., Fournier, J. G., Hauw, J. J., Rossier, J., and Dormont, D. (1997) Transmission of the BSE agent to mice in the absence of detectable abnormal prion protein. *Science 275*, 402–405.
42. Vital, C., Gray, F., Vital, A., Parchi, P., Capellari, S., Petersen, R. B., Ferrer, X., Jarnier, D., Julien, J., and Gambetti, P. (1998) Prion encephalopathy with insertion of octapeptide repeats: The number of repeats determines the type of cerebellar deposits. *Neuropathol. Appl. Neurobiol. 24*, 125–130.
43. Caughey, B., and Lansbury, P. T. (2003) Protofibrils, pores, fibrils, and neurodegeneration: Separating the responsible protein aggregates from the innocent bystanders. *Annu. Rev. Neurosci. 26*, 267–298.
44. Legname, G., Nguyen, H. O., Peretz, D., Cohen, F. E., DeArmond, S. J., and Prusiner, S. B. (2006) Continuum of prion protein structures enciphers a multitude of prion isolate-specified phenotypes. *Proc. Natl. Acad. Sci. U.S.A. 103*, 19105–19110.
45. Moore, R. A., Herzog, C., Errett, J., Kocisko, D. A., Arnold, K. M., Hayes, S. F., and Priola, S. A. (2006) Octapeptide repeat insertions increase the rate of protease-resistant prion protein formation. *Protein Sci. 15*, 609–619.
46. Dong, J., Bloom, J. D., Goncharov, V., Chattopadhyay, M., Millhauser, G. L., Lynn, D. G., Scheibel, T., and Lindquist, S. (2007) Probing the role of PrP repeats in conformational conversion and amyloid assembly of chimeric yeast prions. *J. Biol. Chem. 282*, 34204–34212.
47. Biasini, E., Medrano, A. Z., Thellung, S., Chiesa, R., and Harris, D. A. (2007) Multiple biochemical similarities between infectious and non-infectious aggregates of a prion protein carrying an octapeptide insertion. *J Neurochem 104*, 1293–1308.
48. Silveira, J. R., Raymond, G. J., Hughson, A. G., Race, R. E., Sim, V. L., Hayes, S. F., and Caughey, B. (2005) The most infectious prion protein particles. *Nature 437*, 257–261.
49. Kachel, N., Kremer, W., Zahn, R., and Kalbitzer, H. R. (2006) Observation of intermediate states of the human prion protein by high pressure NMR spectroscopy. *BMC Struct. Biol. 6*, 16.
50. Kaimann, T., Metzger, S., Kuhlmann, K., Brandt, B., Birkmann, E., Holtje, H. D., and Riesner, D. (2007) Molecular model of an α-helical prion protein dimer and its monomeric subunits as derived from chemical cross-linking and molecular modeling calculations. *J. Mol. Biol. 376*, 582–596.
51. Peretz, D., Williamson, R. A., Matsunaga, Y., Serban, H., Pinilla, C., Bastidas, R. B., Rozenshteyn, R., James, T. L., Houghten, R. A., Cohen, F. E., Prusiner, S. B., and Burton, D. R. (1997) A conformational transition at the N terminus of the prion protein features in formation of the scrapie isoform. *J. Mol. Biol. 273*, 614–622.
52. Chen, Y. W., Stott, K., and Perutz, M. F. (1999) Crystal structure of a dimeric chymotrypsin inhibitor 2 mutant containing an inserted glutamine repeat. *Proc. Natl. Acad. Sci. U.S.A. 96*, 1257–1261.
53. Barton, S., Jacak, R., Khare, S. D., Ding, F., and Dokholyan, N. V. (2007) The length dependence of the polyQ-mediated protein aggregation. *J. Biol. Chem. 282*, 25487–25492.
54. Knaus, K. J., Morillas, M., Swietnicki, W., Malone, M., Surewicz, W. K., and Yee, V. C. (2001) Crystal structure of the human prion protein reveals a mechanism for oligomerization. *Nat. Struct. Biol. 8*, 770–774.
55. De Simone, A., Zagari, A., and Derreumaux, P. (2007) Structural and hydration properties of the partially unfolded states of the prion protein. *Biophys. J. 93*, 1284–1292.

BI800253C